

# SPIRIT: Adapting Vision Foundation Models for Unified Single- and Multi-Frame Infrared Small Target Detection

**Qian Xu<sup>1</sup>, Xi Li<sup>1</sup>, Fei Gao<sup>1</sup>, Jie Guo<sup>1</sup>, Haojuan Yuan<sup>4</sup>, Shuaipeng Fan<sup>1</sup> and Mingjin Zhang<sup>1</sup>**

<sup>1</sup>Xidian University

<sup>2</sup>Shanghai Academy of Spaceflight Technology

## Abstract

Infrared small target detection (IRSTD) is crucial for surveillance and early-warning, with deployments spanning both single-frame analysis and video-mode tracking. A practical solution should leverage vision foundation models (VFM) to mitigate infrared data scarcity, while adopting a memory-attention-based temporal propagation framework that unifies single- and multi-frame inference. However, infrared small targets exhibit weak radiometric signals and limited semantic cues, which differ markedly from visible-spectrum imagery. This modality gap makes direct use of semantics-oriented VFM and appearance-driven cross-frame association unreliable for IRSTD: hierarchical feature aggregation can submerge localized target peaks, and appearance-only memory attention becomes ambiguous, leading to spurious clutter associations. To address these challenges, we propose SPIRIT, a unified and VFM-compatible framework that adapts VFM to IRSTD via lightweight physics-informed plug-ins. Spatially, PIFR refines features by approximating rank-sparsity decomposition to suppress structured background components and enhance sparse target-like signals. Temporally, PGMA injects history-derived soft spatial priors into memory cross-attention to constrain cross-frame association, enabling robust video detection while naturally reverting to single-frame inference when temporal context is absent. Experiments on multiple IRSTD benchmarks show consistent gains over VFM-based baselines and SOTA performance.

## 1 Introduction

Infrared small target detection (IRSTD) is a fundamental component of long-range surveillance and early-warning systems, with applications in airborne defense, maritime monitoring, and space situational awareness. In realistic deployments, systems may switch between continuous tracking (video mode) and discrete situational analysis (single-frame mode). This dual requirement motivates a unified detection architecture that works effectively in both regimes and can

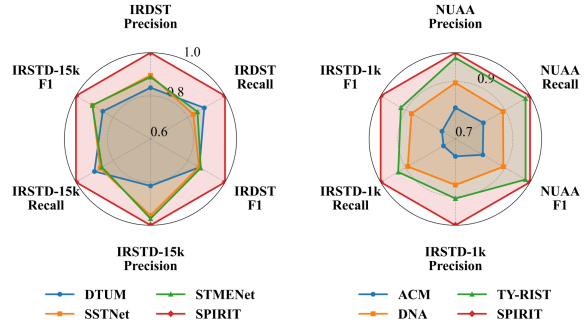


Figure 1: Performance comparison on multi-frame (left) and single-frame (right) IRSTD datasets. All metrics are normalized for clear visualization. Larger enclosed areas indicate superior performance.

gracefully degrade to single-frame inference when temporal information is unavailable. Unlike generic object detection, IRSTD operates in a radiometry-driven regime where targets are tiny and nearly textureless, yet backgrounds are complex and highly structured. As a result, detection depends mostly on subtle intensity contrast; in the video setting, modest but informative motion cues further help, while color, texture, and shape cues are largely absent. Traditional model-driven methods rely on handcrafted priors, such as local contrast or low rank sparse decomposition, but are prone to failure in the presence of strong clutter. Data-driven deep learning methods based on CNNs or Transformers, on the other hand, are often limited by the scarcity of high-quality labeled infrared data. Moreover, most infrared video detectors rely on fixed-clip spatiotemporal models, which are rigid and cannot naturally support both video and single-frame inference within one model. By contrast, memory-attention-based temporal propagation provides a natural route to a unified design: it exploits history when available for video inference, yet naturally reverts to single-frame inference when temporal context is absent. Meanwhile, IRSTD also demands strong generic representations under limited infrared annotations, motivating the use of large-scale pretrained models.

Advances in vision foundation models (VFM), exemplified by SAM Ravi *et al.* [2024] and DINO-style architectures Siméoni *et al.* [2025], are redefining the visual recognition pipeline. Instead of training task-specific backbones from scratch, modern detectors and segmenters increasingly

adapt a single large-scale model pretrained on web-scale RGB images. These VFM<sub>s</sub> provide strong generic features and have demonstrated remarkable transferability across a wide range of downstream tasks, particularly those operating on natural images with rich semantic content. In principle, such models could mitigate data scarcity in IRSTD and offer stronger contextual representations, making the use of VFM<sub>s</sub> as backbones for IRSTD an attractive strategy.

However, directly transplanting these semantics-oriented VFM<sub>s</sub> to the physics-dominated IRSTD domain reveals a fundamental modality mismatch. We identify two critical failure modes where the inductive biases of VFM<sub>s</sub> conflict with the nature of infrared imaging: **(i) Spatial feature submergence.** Hierarchical backbones progressively aggregate information through deep token mixing and large effective receptive fields. While this benefits semantic coherence in natural images, IR small targets manifest as weak, localized intensity singularities occupying only a few pixels, often embedded in structured clutter such as cloud edges or sea waves. Under repeated aggregation, such small peaks are easily diluted and overshadowed by strong background responses. Consequently, the signal-to-clutter ratio (SCR) of valid targets collapses in deeper layers, leading to missed detections. **(ii) Temporal appearance ambiguity.** Along the temporal dimension, Transformers and memory-attention-based architectures typically perform association by matching appearance features across frames, which is effective when objects have distinctive semantic attributes. However, in infrared sequences, small targets are nearly textureless. Their appearance is inherently ambiguous and often indistinguishable from dynamic clutter. A global, appearance-only attention mechanism is therefore under-constrained and cannot reliably query the correct target from memory, forming spurious associations between high-response background patterns and the target trajectory that amplify false alarms and degrade detection stability. In short, semantics-driven representations tend to dilute weak local peaks spatially and become unreliable for appearance-based association temporally.

To address these challenges, we propose SPIRIT (Spatiotemporal Physics-Informed Representation for Infrared Targets), a unified framework that adapts semantics-oriented VFM<sub>s</sub> to IRSTD by injecting physically motivated constraints into feature representation and attention, in a backbone-compatible manner and without redesigning the pretrained VFM. The proposed modules are lightweight plugins that can be integrated into different VFM backbones with minimal changes. On the spatial side, we introduce a Physics-Informed Feature Refinement (PIFR) that acts as a differentiable physical filter inside the encoder. PIFR approximates rank-sparsity decomposition in the feature domain, suppressing low-rank background components and enhancing sparse target-like responses, thereby alleviating feature submergence without sacrificing the benefits of large-scale pretraining. On the temporal side, we design a Prior-Guided Memory Attention (PGMA) mechanism that injects a feasibility prior into memory cross-attention: cues distilled from previous-frame detections are encoded as a soft spatial prior and used to bias the attention toward plausible associations. This converts unconstrained global appearance match-

ing into feasibility-guided local matching, suppressing clutter that is visually similar but spatially implausible. SPIRIT operates in both single-frame and video regimes, and when temporal information is unavailable it naturally falls back to a purely spatial detector, enabling flexible deployment under dynamic operational requirements.

Our main contributions are summarized as follows:

- We propose SPIRIT, a unified and VFM-compatible framework that injects physics-informed plug-ins into semantics-oriented VFM<sub>s</sub>, supports both single-frame and video IRSTD, and gracefully degrades to single-frame inference when temporal cues are unavailable.
- We introduce PIFR, a differentiable rank-sparsity decomposition refinement module that suppresses structured backgrounds and enhances sparse targets to mitigate feature submergence.
- We design PGMA, a prior-guided memory attention mechanism that leverages history-derived spatial priors to constrain cross-frame association, reducing spurious matches and improving detection stability.
- Extensive experiments on IRSTD benchmarks demonstrate that SPIRIT consistently improves VFM-based baselines and achieves SOTA performance.

## 2 Related Work

**Single-frame IR Small Target Detection.** Early IRSTD mainly relied on model-driven priors such as local contrast and low-rank/sparse decomposition Gao *et al.* [2013]; Zhang *et al.* [2018]; Dai and Wu [2017], which are interpretable but fragile under strong structured clutter. Recent CNN/Transformer detectors Dai *et al.* [2021]; Li *et al.* [2022]; Zhang *et al.* [2025a] learn features end-to-end and achieve notable gains, yet they are typically trained from scratch on scarce infrared annotations, limiting generalization. This motivates transferring pretrained VFM<sub>s</sub> to IRSTD.

**Video IRSTD and Temporal Association.** Temporal cues help suppress clutter via motion consistency; classical pipelines use flow compensation or temporal filtering. Deep video IRSTD models Yan *et al.* [2023]; Tong *et al.* [2024]; Chen *et al.* [2024] aggregate multi-frame features with 3D convolutions or spatiotemporal attention, but many operate on fixed-length clips and cannot gracefully degrade to single-frame inference. Moreover, generic video detectors often associate frames by appearance similarity, which is under-constrained for textureless infrared targets and easily confused by dynamic clutter, motivating feasibility-guided temporal matching beyond appearance-only attention.

**Vision Foundation Models and Adaptation.** Vision foundation models (VFM<sub>s</sub>) such as SAM Ravi *et al.* [2024] and DINO-style models Siméoni *et al.* [2025] provide transferable representations widely used for downstream vision tasks. Parameter-efficient fine-tuning methods including LoRA, adapters, and prompt tuning enable efficient adaptation. Recent works have explored transferring VFM<sub>s</sub> to infrared small-target tasks Zhang *et al.* [2024, 2025b], but also report that direct transfer can be unstable in cluttered scenes

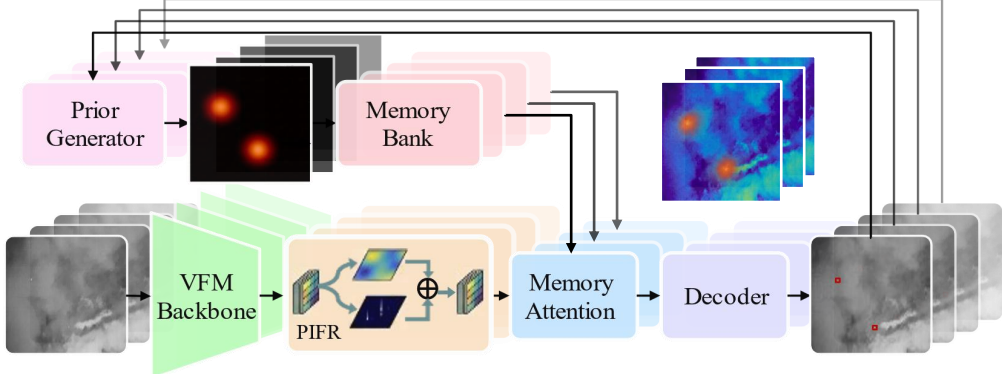


Figure 2: The overall architecture of the proposed method. It integrates PIFR into the VFM backbone to decouple background and target for feature enhancement, and employs prior guided memory attention to suppress spurious associations by leveraging a feasibility field to focus on physically plausible regions.

with limited gains due to the modality gap. Thus, effective VFM adaptation for IRSTD likely requires task-aware designs beyond routine fine-tuning.

### 3 Method

**Overview.** The overall architecture of SPIRIT is illustrated in Figure 2. It is built upon a hierarchical VFM backbone to extract multi-scale feature pyramids. To mitigate feature submergence, which typically intensifies during deep feature aggregation, we strategically insert the PIFR module into the last two backbone stages. This placement allows the model to explicitly restore sparse target signals in high-level semantic features before they are overwhelmed by the background. For video inputs, these refined features serve as queries for the PGMA mechanism to suppress spurious associations via history-constrained interaction. Finally, to translate the refined representations into detections, we adopt the lightweight decoder from DEIM Huang *et al.* [2025]. We preserve its core design and only modify the interface to align VFM tokens, ensuring a fair comparison while inheriting its high inference efficiency.

#### 3.1 Physics-Informed Feature Refinement

Infrared small targets appear as weak sparse spikes, whereas backgrounds become globally coherent after VFM aggregation. This discrepancy causes feature submergence, where target peaks are overwhelmed by deep token mixing. To explicitly disentangle sparse targets from coherent backgrounds, we introduce Physics-Informed Feature Refinement (Figure 3). This lightweight plug-in approximates a rank-sparsity decomposition to recover target cues and injects them back via an identity-preserving residual.

Let  $X_{\text{in}} \in \mathbb{R}^{C \times H \times W}$  be a deep feature map and  $\bar{X} \in \mathbb{R}^{C \times N}$  ( $N = HW$ ) its spatially flattened form. Following a standard infrared prior, we model

$$\bar{X} = B + T + N, \quad (1)$$

where  $B$  denotes structured background/clutter,  $T$  denotes sparse target-like responses, and  $N$  denotes residual noise. Classical RPCA estimates  $B$  via iterative SVD, which is

costly and inconvenient to integrate into modern VFM backbones. Instead, we exploit an empirical spectral property of infrared backgrounds: after deep aggregation, clutter responses are dominated by a few globally correlated components, yielding a rapidly decaying singular-value spectrum Gao *et al.* [2013]; Zhang *et al.* [2018]. We thus approximate the background by a fixed low-rank subspace of rank  $r$  (we use  $r = 4$  throughout, as most background energy concentrates in the leading singular directions),

$$B \approx UV^T, \quad \text{rank}(B) \leq r. \quad (2)$$

To avoid explicit SVD, we construct coarse background prototypes via spatial pooling. Let  $M \in \mathbb{R}^{N \times r}$  be a fixed pooling matrix whose columns correspond to  $r$  non-overlapping coarse spatial bins, normalized to average features within each bin. We compute pooled prototypes

$$G = \bar{X}M \in \mathbb{R}^{C \times r}, \quad (3)$$

map  $G$  to a background basis  $U = \phi(G) \in \mathbb{R}^{C \times r}$  using a lightweight projector  $\phi(\cdot)$ , and estimate the low-rank background by a closed-form ridge projection,

$$\hat{B} = U(U^T U + \delta I)^{-1} U^T \bar{X}, \quad (4)$$

where  $\delta$  is a small constant for numerical stability and  $I$  is the  $r \times r$  identity. This operation is SVD-free and lightweight, requiring only an  $r \times r$  matrix inverse. We then form the residual  $R = \bar{X} - \hat{B}$ , which contains sparse/high-frequency components where small targets are expected to reside. To extract target-like responses while suppressing diffuse noise, we apply a token-wise group shrinkage,

$$T_{:,i} = \max\left(1 - \frac{\text{softplus}(\rho)}{\|R_{:,i}\|_2 + \epsilon}, 0\right) R_{:,i}, \quad i = 1, \dots, N, \quad (5)$$

where  $\rho$  is learnable and  $\epsilon$  is a small constant. Using  $\text{softplus}(\rho)$  ensures a positive shrinkage threshold and stabilizes optimization: locations with small  $\ell_2$  magnitude across channels are attenuated, while sparse peaks with large magnitude are preserved. We then convert sparsity into a soft gate by

$$S = \text{reshape}(\{\|T_{:,i}\|_2\}_{i=1}^N), \quad m = \sigma(\text{Conv}(S)), \quad (6)$$

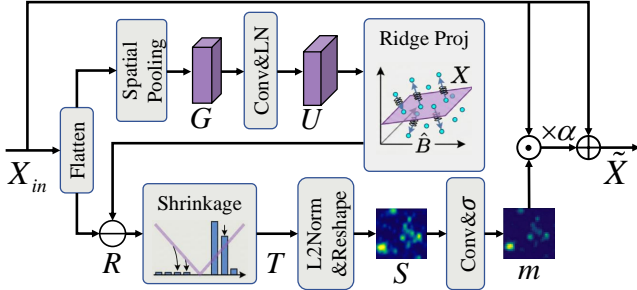


Figure 3: Illustration of the PIFR module, which utilizes ridge projection and shrinkage for feature refinement.

and refine features in an identity-preserving residual form:

$$\tilde{X} = X_{in} + \alpha (X_{in} \odot m), \quad (7)$$

where  $\odot$  denotes element-wise multiplication and  $\alpha$  is a learnable scale initialized to 0. This initialization preserves the pretrained backbone at early training stages while gradually introducing the physical prior, improving stability when adapting large VFM to the infrared domain. Overall, PIFR counteracts feature submergence by suppressing globally coherent clutter and enhancing sparse target evidence, while introducing minimal overhead dominated, making it practical for integration into diverse hierarchical VFM backbones.

### 3.2 Prior-Guided Memory Attention

Infrared video small targets are extremely small and often textureless; consequently, appearance similarity alone is unreliable for temporal association. Meanwhile, dynamic clutter can produce target-like responses across frames, so unconstrained memory retrieval based purely on global appearance matching may form spurious associations. Worse, such mistakes can be progressively reinforced through the recurrent write-read cycle of a memory bank, leading to temporal drift and persistent false alarms. To mitigate this IR-specific failure mode, we propose Prior-Guided Memory Attention (PGMA), which formulates temporal association as feasibility-constrained memory retrieval with a prior-gated memory encoding. When the memory is empty or the feasibility prior degenerates to uniform, PGMA naturally reduces to standard cross-attention, unifying single-frame and video inference without additional branches.

The refined deepest feature  $\tilde{X}_t^{(L)} \in \mathbb{R}^{C \times H_L \times W_L}$  is adopted as the carrier for temporal interaction, flattened into  $N = H_L W_L$  tokens to serve as current-frame queries. To construct a continuous and differentiable feasibility prior, previous-frame detections  $\mathcal{D}_{t-1} = \{(b_{t-1}^{(m)}, s_{t-1}^{(m)})\}_{m=1}^{M_{t-1}}$  are utilized, where  $b^{(m)} = (x_1, y_1, x_2, y_2)$ . Each box is mapped to the deep grid to yield its center  $c^{(m)}$  and scale  $r^{(m)}$ , from which a multi-peak feasibility field is generated:

$$G_{t-1}(p) = \sum_{m=1}^{M_{t-1}} \exp\left(-\frac{\|p - c^{(m)}\|_2^2}{2\kappa^2(r^{(m)})^2}\right), \quad (8)$$

where  $p$  denotes a grid location and  $\kappa$  controls the tolerated search radius. This representation naturally supports an unknown number of targets via a soft union of peaks. When no

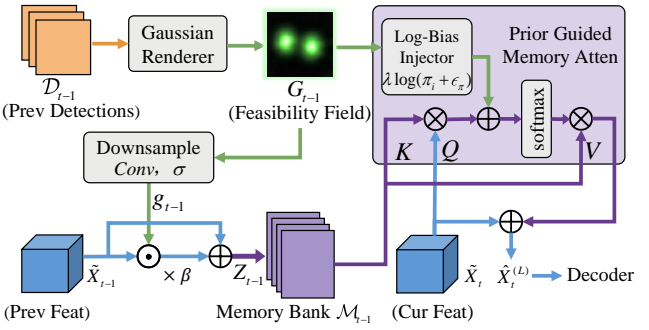


Figure 4: The workflow of PGMA. By utilizing a Gaussian feasibility field as a prior for gated encoding and bias injection, this mechanism guides the model to focus on physically plausible regions to suppress spurious associations.

reliable detection exists ( $M_{t-1} = 0$ ), we set  $G_{t-1}(p) \equiv 1$ , so the prior degenerates to uniform and does not block newly appearing targets.

$G_{t-1}$  is downsampled to match the resolution of  $\tilde{X}_{t-1}^{(L)}$ , yielding a lightweight gate map:

$$g_{t-1} = \sigma(\text{Conv}_{3 \times 3}(\text{Down}(G_{t-1}))) \in [0, 1]^{1 \times H_L \times W_L}, \quad (9)$$

which modulates the memory feature through a gated residual encoding:

$$Z_{t-1} = \tilde{X}_{t-1}^{(L)} + \beta(\tilde{X}_{t-1}^{(L)} \odot g_{t-1}), \quad (10)$$

where  $\odot$  is element-wise multiplication and  $\beta$  is a learnable scale initialized to 0 to inherit pretrained representations stably.  $Z_{t-1}$  is written into the memory bank  $\mathcal{M}_{t-1}$ , and the grid coordinate  $P_i$  is recorded for each spatial location to enable prior evaluation during addressing. The memory bank  $\mathcal{M}_{t-1}$  stores spatial memories from the most recent  $K$  frames in a FIFO manner.

At read time, PGMA performs cross-attention from the memory bank: queries  $q_j$  come from the current frame tokens, and keys/values ( $k_i, v_i$ ) come from memory entries. We take appearance similarity as the base score and introduce the feasibility prior as a log-bias. Let  $\pi_i = G_{t-1}(P_i)$  be the feasibility weight at the memory position  $P_i$ . The prior-guided logits and attention weights are:

$$s'_{j,i} = \frac{q_j^\top k_i}{\sqrt{d}} + \lambda \log(\pi_i + \epsilon_\pi), \quad w_{j,i} = \text{softmax}_i(s'_{j,i}), \quad (11)$$

where  $\epsilon_\pi$  is a numerical stabilizer. Rather than tuning hyperparameters, we learn the prior strength via a bounded parameterization:

$$\lambda = \lambda_{\max} \sigma(\theta_\lambda). \quad (12)$$

For training stability, we initialize  $\theta_\lambda$  to a negative value so that  $\lambda$  start small. When  $\pi_i$  is small, the bias suppresses attention to physically implausible locations, reducing spurious associations caused by appearance ambiguity. Crucially, this soft-constraint mechanism also prevents error accumulation from false alarms (FP): even if an FP induces a misleading spatial bias, the low appearance similarity of suppressed

Method	Venue	IRDST				IRSTD-15k				Params	FLOPs	FPS
		AP50	P	R	F1	AP50	P	R	F1			
DTUM	TNNLS’2023	71.48	82.87	87.79	85.26	67.97	77.95	88.28	82.79	<b>9.6</b>	128.2	13.9
TMP	ESA’2024	70.01	86.65	81.36	83.92	77.73	92.97	84.74	88.67	16.4	92.9	25.0
SSTNet	TGRS’2024	71.55	88.56	81.92	85.11	76.96	91.05	85.29	88.07	11.9	123.6	22.6
Tridos	TGRS’2024	73.72	84.49	89.35	86.85	80.41	90.71	90.60	90.65	14.1	130.7	13.7
STMENet	ESA’2025	73.40	87.78	84.22	85.96	77.33	92.42	84.35	88.21	<u>10.4</u>	<b>45.8</b>	<u>48.5</u>
MOCID	AAAI’2025	94.74	<b>98.92</b>	96.86	97.88	86.84	90.37	92.44	91.40	13.1	98.7	11.5
TDCNet	AAAI’2025	<u>94.79</u>	98.12	<u>97.71</u>	<u>97.91</u>	<u>88.17</u>	<u>94.50</u>	<u>96.75</u>	<u>95.61</u>	24.8	95.7	18.5
SPIRIT	–	<b>96.24</b>	<u>98.91</u>	<b>98.26</b>	<b>98.58</b>	<b>89.56</b>	<b>95.34</b>	<b>97.15</b>	<b>96.23</b>	32.2	<u>65.6</u>	<b>53.1</b>

Table 1: Comparison on multi-frame benchmarks (IRDST and IRSTD-15k). The best results are highlighted in bold and the second-place results are highlighted in underline.

background features (via PIFR) counteracts the bias, preventing the solidification of a false trajectory. Finally, we read memory values and fuse them back to current tokens in a residual form:

$$\hat{q}_j = q_j + \gamma \sum_i w_{j,i} v_i, \quad \hat{X}_t^{(L)} = \text{reshape}(\{\hat{q}_j\}_{j=1}^N), \quad (13)$$

where  $\gamma$  is a learnable scale initialized to a small value. The decoder always receives the memory-conditioned current-frame feature  $\hat{X}_t^{(L)}$ . This architecture ensures robustness to missed detections (FN): when the memory is empty or an FN occurs ( $G_{t-1}(p) \equiv 1$ ), PGMA naturally reverts to global content-based retrieval. This allows the model to recover targets from longer-term history based on appearance cues, ensuring graceful degradation.

## 4 Experiments

### 4.1 Datasets and Evaluation Metrics

**Datasets.** For our experiments, we evaluate the performance of our method using both single-frame and multi-frame datasets. The single-frame datasets used are NUAA-SIRST Dai *et al.* [2021], IRSTD-1k Zhang *et al.* [2022], and NUDT-SIRST Li *et al.* [2022]. For multi-frame tracking, we use the IRDST Sun *et al.* [2023] and IRSTD-15k Duan *et al.* [2024] datasets.

**Evaluation Metrics** For evaluation, we adopt standard metrics, including precision (P), recall (R), F1-score (F1), and average precision (AP50), all computed at an intersection-over-union (IoU) threshold of 0.5. Real-time performance is measured in frames per second (FPS), while computational complexity is assessed using the number of parameters (Params) and floating point of operations (FLOPs).

### 4.2 Implementation Details

The algorithm is implemented in PyTorch and utilizes the AdamW optimizer with  $\beta$  values set to [0.9, 0.999]. For parameters related to the dinov3 backbone network, the learning rate is set to  $1 \times 10^{-5}$  and weight decay is set to  $1 \times 10^{-4}$ . For other parts of the model, the optimizer’s learning rate is set to  $5 \times 10^{-4}$  and weight decay is set to 0.000125. For all experiments, the input frames are resized to  $512 \times 512$  pixels.

Unless stated otherwise, we use DINOv3 ViT-S for the backbone and K=5 for the memory length in multi-frame settings. The batch size is 24, and the training runs for 50 epochs. To supervise the training, we employ bbox loss (L1), GIoU loss Rezatofighi *et al.* [2019], and cls Loss. The total loss is given by:  $L = \lambda_1 \cdot L_{\text{bbox}} + \lambda_2 \cdot L_{\text{cls}} + \lambda_3 \cdot L_{\text{GIoU}}$  where the ratio of the coefficients is set to 2:1:1. Training is performed using two RTX 3090 GPUs, and testing is conducted with a single RTX 3090 GPU. For single-frame methods, we include ACM Dai *et al.* [2021], ISNet Zhang *et al.* [2022], DNANet Li *et al.* [2022], UIUNet Wu *et al.* [2022], AGPCNet Zhang *et al.* [2023], PConv Yang *et al.* [2025] and TY-RIST Atrash *et al.* [2025]. For multi-frame methods, we include DTUM Li *et al.* [2023], TMP Zhu *et al.* [2024], SSTNet Chen *et al.* [2024], STMENet Peng *et al.* [2025], MOCID Zhang *et al.* [2025c] and TDCNet Fang *et al.* [2025]

### 4.3 Main Results

**Multi-frame benchmarks.** Table 1 reports results on two multi-frame benchmarks, IRDST and IRSTD-15k. SPIRIT consistently outperforms previous methods across all metrics. Compared with the strongest prior competitor, SPIRIT achieves notable improvements in both AP50 and F1-score on IRDST. On IRSTD-15k, our method further secures a clear performance lead, demonstrating higher precision and recall compared to existing approaches. In videos, SPIRIT benefits from the joint effect of two complementary components: PIFR enhances sparse target evidence while suppressing globally consistent clutter in the feature domain, and PGMA converts under-constrained appearance matching into feasibility-constrained memory retrieval with confidence-gated updates. Their combination yields more stable detections under infrared appearance ambiguity, reducing spurious associations and preventing error reinforcement over time.

**Single-frame benchmarks.** Table 2 compares SPIRIT with representative CNN-based IRSTD detectors on IRSTD-1k, NUAA-SIRST, and NUDT-SIRST. SPIRIT achieves state-of-the-art performance across the evaluated metrics, indicating that the proposed physics-informed feature refinement effectively alleviates feature submergence of tiny, low-SCR targets under structured clutter. Notably, the consistently high F1 scores suggest that our method maintains a favorable balance between precision and recall, which is crucial in IRSTD

Method	Venue	NUAA-SIRST			NUDT-SIRST			IRSTD-1k			Params	FLOPs	FPS
		P	R	F1	P	R	F1	P	R	F1			
ACM	WACV’2021	76.5	76.2	76.3	73.2	74.5	73.8	67.9	60.5	64.0	3.0	<b>24.7</b>	29.1
ISNet	CVPR’2022	82.0	84.7	83.4	74.2	83.4	78.5	71.8	74.1	72.9	3.5	265.7	10.2
DNA Net	TIP’2022	84.7	83.6	84.1	91.4	88.9	90.1	76.8	72.1	74.4	7.2	135.2	7.8
UIUNet	TIP’2022	93.4	88.4	90.8	97.2	91.8	94.4	85.7	79.5	82.5	53.1	456.7	3.6
IRSAM	ECCV’2024	89.4	88.7	89.1	95.1	93.4	94.2	79.6	80.2	79.9	12.3	76.1	7.4
AGPCNet	TAES’2023	39.0	81.0	52.7	36.8	68.4	47.9	41.5	47.0	44.1	14.9	366.2	4.8
PConv	AAAI’2025	<b>97.1</b>	89.0	<u>92.9</u>	<u>98.0</u>	94.7	<u>96.4</u>	86.7	<b>80.9</b>	<u>83.7</u>	23.8	88.6	58.8
TY-RIST	ICCV’2025	92.9	<u>92.1</u>	92.5	96.8	<b>95.8</b>	96.3	81.0	75.2	78.0	<b>2.03</b>	37.4	<b>123.1</b>
SPIRIT	–	94.6	<b>93.8</b>	<b>94.2</b>	<b>98.3</b>	94.7	<b>96.5</b>	<b>89.3</b>	<b>80.9</b>	<b>84.9</b>	32.2	63.7	60.1

Table 2: Comparison on single-frame benchmarks (NUAA-SIRST, NUDT-SIRST and IRSTD-1k). The best results are highlighted in bold and the second-place results are highlighted in underline.

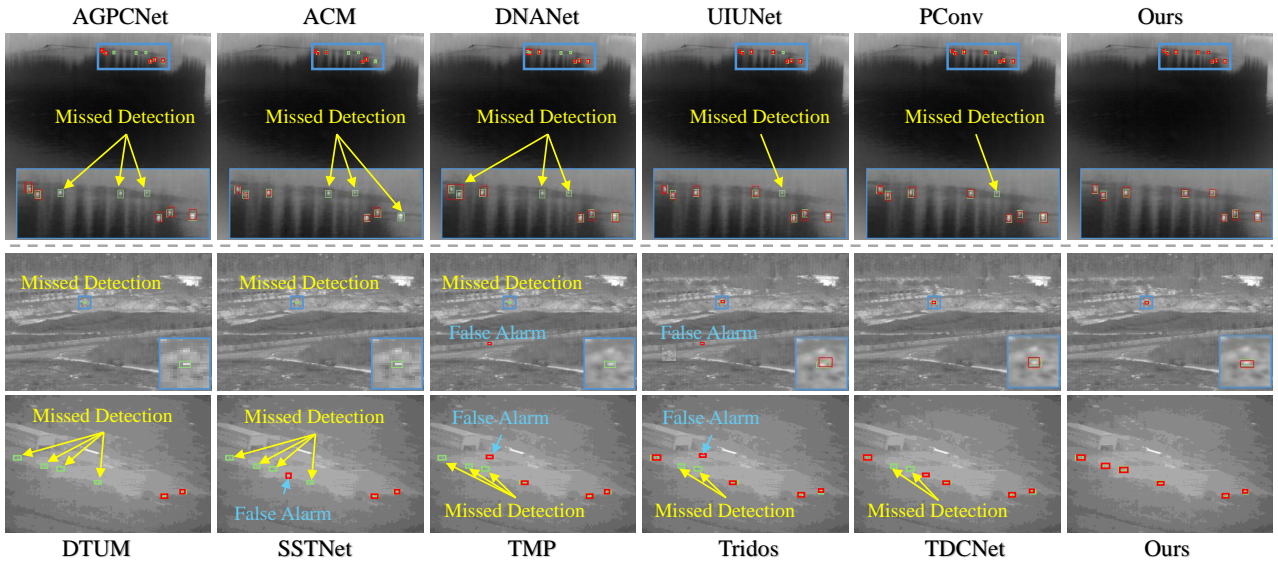


Figure 5: Visual comparison of results from different methods on the IRSTD-1k, IRDST, and IRSTD-15k datasets. Boxes in green and red represent ground-truth and detected targets, respectively.

where both clutter-induced false alarms and missed detections are common.

**Qualitative Results** Figure 5 provides qualitative comparisons on representative single-frame and multi-frame IRSTD scenes. Overall, competing methods exhibit typical failure modes in infrared imagery, including missed detections under low-SCR targets, clutter-induced false alarms, and imprecise localization. In contrast, SPIRIT yields more complete detections with fewer spurious responses and tighter boxes, consistent with the quantitative results. In the single-frame case with multiple targets, several baselines miss at least one target, whereas SPIRIT detects all targets. In the multi-frame single-target case, baselines either miss the target, trigger false alarms, or show less accurate boxes, while SPIRIT maintains stable detection and tighter localization. In the multi-frame multi-target case, baselines suffer from misses or false alarms and degraded localization under multiple distractors, whereas SPIRIT detects all targets with fewer false positives and more precise boxes.

#### 4.4 Ablation Study

**Impact of the proposed PIFR and PGMA.** Table 3 validates the contribution of each component. The Baseline suffers from feature submergence, resulting in suboptimal Recall. The integration of PIFR yields a substantial improvement in Recall, validating that the physics-informed shrinkage effectively recovers submerged sparse targets from deep features. Conversely, PGMA primarily enhances Precision by leveraging temporal feasibility priors to filter out physically implausible dynamic clutter. The best performance is achieved when both modules work in synergy. Furthermore, our proposed framework significantly outperforms the standard Adapter. While the Adapter provides marginal gains through generic domain adaptation, it relies on implicit feature remapping and lacks specific inductive biases for small targets. In contrast, our approach explicitly models the physical characteristics of background low-rankness and temporal feasibility, proving more effective than generic adapters in addressing the fundamental challenges of feature submergence

Setting	AP50	P	R	F1
Baseline	86.21	91.44	89.37	90.39
+ Adapter	86.85	92.15	90.82	91.48
+ PIFR	<u>88.62</u>	93.28	<u>96.55</u>	<u>94.89</u>
+ PGMA	87.14	94.62	89.95	92.23
+ Adapter + PGMA	87.90	<u>95.10</u>	91.35	93.19
+ PIFR + PGMA	<b>89.56</b>	<b>95.34</b>	<b>97.15</b>	<b>96.23</b>

Table 3: Ablation study on IRSTD-15k. “Adapter” denotes the standard parameter-efficient fine-tuning module proposed by Houlsby *et al.* [2019].

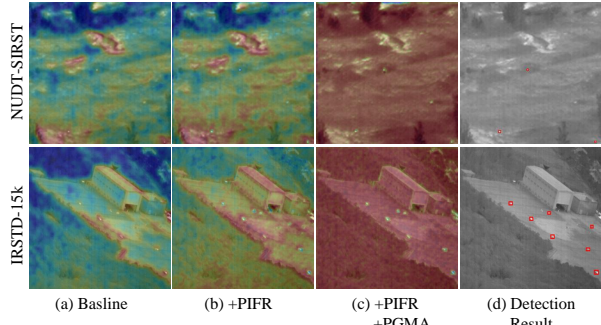


Figure 6: Heat map visualization illustrating the progressive enhancement achieved by PIFR and PGMA.

and appearance ambiguity.

Figures 6 show feature visualizations for single-frame and multi-frame scenarios. In the single-frame case, applying PIFR clearly enhances target features, making them more salient and less affected by clutter. PGMA has little effect on single-frame detection, keeping performance stable without temporal context. For multi-frame sequences, PGMA helps filter spurious targets and reduce false positives, as reflected in the visualizations. Target features become clearer, and the model better separates real targets from background clutter. This indicates PGMA effectively stabilizes temporal associations and suppresses tracking errors, resulting in more robust and accurate video detection.

**Impact of the memory length  $K$ .** We investigate the sensitivity of SPIRIT to the memory length  $K$  by varying  $K \in \{1, 3, 5, 7, 9\}$  while keeping the input resolution fixed. Figure 7 shows that increasing  $K$  from 1 to a moderate value consistently improves performance, indicating that retaining short-term history benefits feasibility-constrained retrieval under infrared appearance ambiguity. However, when  $K$  becomes too large, the performance saturates and can even drop. This trend is consistent with PGMA: moderate memory provides relevant recent evidence to recover weak targets across frames, whereas an overly long memory introduces a larger pool of older key-value tokens that are less relevant to the current frame. Since infrared backgrounds are highly non-stationary, stale memories may contain outdated clutter patterns that remain visually target-like and act as strong distractors during retrieval. We therefore set  $K = 5$  by default as a good trade-off between accuracy and efficiency.

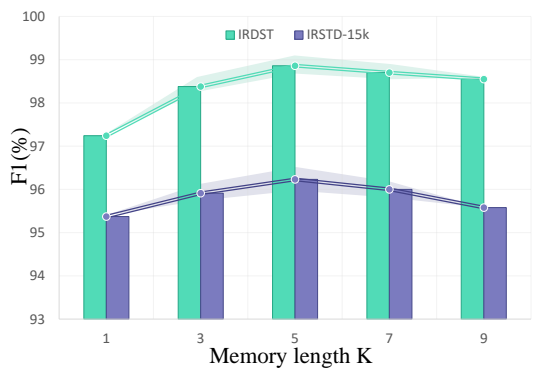


Figure 7: Sensitivity to memory length  $K$  on multi-frame datasets.

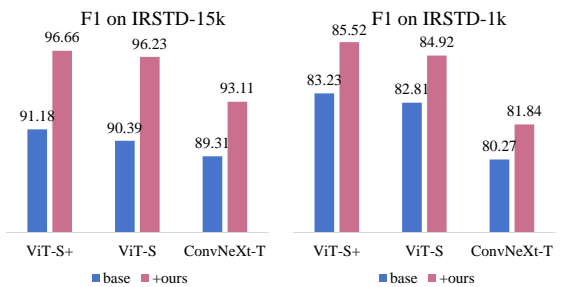


Figure 8: Performance comparison across different backbones.

**Generalization across Backbones.** To verify the universality of our framework, we evaluate the proposed method with three different backbones: DINOv3-based ViT-S+, ViT-S, and ConvNeXt-T, on both IRSTD-15k and IRSTD-1k datasets. As shown in Figure 8, performance naturally improves with stronger backbones. Integrating our proposed modules yields consistent and significant improvements across all architectures. This demonstrates that our method is not reliant on a specific backbone but addresses the limitations of deep features in IRSTD, providing a robust plug-and-play solution for diverse foundation models.

## 5 Conclusion

In this work, we propose SPIRIT, a unified framework that adapts Vision Foundation Models for robust infrared small target detection. The proposed approach overcomes the limitations of generic semantic features through two lightweight, physics-inspired plug-ins. Specifically, PIFR mitigates feature submergence by approximating a rank-sparsity decomposition to enhance target discriminability, while PGMA resolves appearance ambiguity by injecting spatial feasibility priors into memory attention. This design enables a single model to handle both video and single-frame inputs effectively. Experimental results across multiple benchmarks confirm that SPIRIT significantly outperforms existing baselines and state-of-the-art methods, validating the effectiveness of embedding physical constraints into large-scale pretrained backbones.

## References

- Abdulkarim Atrash, Seyda Ertekin, Omur Ugur, Omar Moured, Yufan Chen, and Jiaming Zhang. Ty-rist: Tactical yolo tricks for real-time infrared small target detection. In *Proceedings of the IEEE/CVF International Conference on Computer Vision*, pages 2201–2210, 2025.
- Shengjia Chen, Luping Ji, Jiewen Zhu, Mao Ye, and Xiaoyong Yao. Sstnet: Sliced spatio-temporal network with cross-slice convlstm for moving infrared dim-small target detection. *IEEE Transactions on Geoscience and Remote Sensing*, 62:1–12, 2024.
- Yimian Dai and Yiquan Wu. Reweighted infrared patch-tensor model with both nonlocal and local priors for single-frame small target detection. *IEEE journal of selected topics in applied earth observations and remote sensing*, 10(8):3752–3767, 2017.
- Yimian Dai, Yiquan Wu, Fei Zhou, and Kobus Barnard. Asymmetric contextual modulation for infrared small target detection. In *Proceedings of the IEEE/CVF winter conference on applications of computer vision*, pages 950–959, 2021.
- Weiwei Duan, Luping Ji, Shengjia Chen, Sicheng Zhu, and Mao Ye. Triple-domain feature learning with frequency-aware memory enhancement for moving infrared small target detection. *IEEE Transactions on Geoscience and Remote Sensing*, 2024.
- Houzhang Fang, Shukai Guo, Qiuhan Chen, Yi Chang, and Luxin Yan. Spatio-temporal context learning with temporal difference convolution for moving infrared small target detection. *arXiv preprint arXiv:2511.09352*, 2025.
- Chenqiang Gao, Deyu Meng, Yi Yang, Yongtao Wang, Xiaofang Zhou, and Alexander G Hauptmann. Infrared patch-image model for small target detection in a single image. *IEEE transactions on image processing*, 22(12):4996–5009, 2013.
- Neil Houlsby, Andrei Giurgiu, Stanislaw Jastrzebski, Bruna Morrone, Quentin De Laroussilhe, Andrea Gesmundo, Mona Attariyan, and Sylvain Gelly. Parameter-efficient transfer learning for nlp. In *International Conference on Machine Learning (ICML)*, pages 2790–2799. PMLR, 2019.
- Shihua Huang, Zhichao Lu, Xiaodong Cun, Yongjun Yu, Xiao Zhou, and Xi Shen. Deim: Detr with improved matching for fast convergence. In *Proceedings of the Computer Vision and Pattern Recognition Conference*, pages 15162–15171, 2025.
- Boyang Li, Chao Xiao, Longguang Wang, Yingqian Wang, Zaiping Lin, Miao Li, Wei An, and Yulan Guo. Dense nested attention network for infrared small target detection. *IEEE Transactions on Image Processing*, 32:1745–1758, 2022.
- Ruojing Li, Wei An, Chao Xiao, Boyang Li, Yingqian Wang, Miao Li, and Yulan Guo. Direction-coded temporal u-shape module for multiframe infrared small target detection. *IEEE Transactions on Neural Networks and Learning Systems*, 2023.
- Shuang Peng, Luping Ji, Shengjia Chen, Weiwei Duan, and Sicheng Zhu. Moving infrared dim and small target detection by mixed spatio-temporal encoding. *Engineering Applications of Artificial Intelligence*, 144:110100, 2025.
- Nikhila Ravi, Valentin Gabeur, Yuan-Ting Hu, Ronghang Hu, Chaitanya Ryali, Tengyu Ma, Haitham Khedr, Roman Rädl, Chloe Rolland, Laura Gustafson, et al. Sam 2: Segment anything in images and videos. *arXiv preprint arXiv:2408.00714*, 2024.
- Hamid Rezatofighi, Nathan Tsoi, JunYoung Gwak, Amir Sadeghian, Ian Reid, and Silvio Savarese. Generalized intersection over union: A metric and a loss for bounding box regression. In *Proceedings of the IEEE/CVF conference on computer vision and pattern recognition*, pages 658–666, 2019.
- Oriane Siméoni, Huy V Vo, Maximilian Seitzer, Federico Baldassarre, Maxime Oquab, Cijo Jose, Vasil Khalidov, Marc Szafraniec, Seungeun Yi, Michaël Ramamonjisoa, et al. Dinov3. *arXiv preprint arXiv:2508.10104*, 2025.
- Heng Sun, Junxiang Bai, Fan Yang, and Xiangzhi Bai. Receptive-Field and Direction Induced Attention Network for Infrared Dim Small Target Detection With a Large-Scale Dataset IRDST. *IEEE Transactions on Geoscience and Remote Sensing*, 61:1–13, 2023.
- Xiaozhong Tong, Zhen Zuo, Shaojing Su, Junyu Wei, Xiaoyong Sun, Peng Wu, and Zongqing Zhao. St-trans: Spatial-temporal transformer for infrared small target detection in sequential images. *IEEE Transactions on Geoscience and Remote Sensing*, 62:1–19, 2024.
- Xin Wu, Danfeng Hong, and Jocelyn Chanussot. UIU-Net: U-Net in U-Net for infrared small object detection. *IEEE Transactions on Image Processing*, 32:364–376, 2022.
- Puti Yan, Runze Hou, Xuguang Duan, Chengfei Yue, Xin Wang, and Xibin Cao. STDMANet: Spatio-temporal differential multiscale attention network for small moving infrared target detection. *IEEE Transactions on Geoscience and Remote Sensing*, 61:1–16, 2023.
- Jiangnan Yang, Shuangli Liu, Jingjun Wu, Xinyu Su, Nan Hai, and Xueli Huang. Pinwheel-shaped convolution and scale-based dynamic loss for infrared small target detection. In *Proceedings of the AAAI Conference on Artificial Intelligence*, volume 39, pages 9202–9210, 2025.
- Landan Zhang, Lingbing Peng, Tianfang Zhang, Siying Cao, and Zhenming Peng. Infrared small target detection via non-convex rank approximation minimization joint 1 2, 1 norm. *Remote Sensing*, 10(11):1821, 2018.
- Mingjin Zhang, Rui Zhang, Yuxiang Yang, Haichen Bai, Jing Zhang, and Jie Guo. Isnet: Shape matters for infrared small target detection. In *Proceedings of the IEEE/CVF conference on computer vision and pattern recognition*, pages 877–886, 2022.
- Tianfang Zhang, Lei Li, Siying Cao, Tian Pu, and Zhenming Peng. Attention-guided pyramid context networks for detecting infrared small target under complex background. *IEEE Transactions on Aerospace and Electronic Systems*, 59(4):4250–4261, 2023.

Mingjin Zhang, Yuchun Wang, Jie Guo, Yunsong Li, Xinbo Gao, and Jing Zhang. Irsam: Advancing segment anything model for infrared small target detection. In *European Conference on Computer Vision*, pages 233–249. Springer, 2024.

Mingjin Zhang, Xiaolong Li, Fei Gao, and Jie Guo. IR-Mamba: Pixel difference mamba with layer restoration for infrared small target detection. In *AAAI Conference on Artificial Intelligence*, volume 39, pages 10003–10011, 2025.

Mingjin Zhang, Xiaolong Li, Fei Gao, Jie Guo, Xinbo Gao, and Jing Zhang. Saist: Segment any infrared small target model guided by contrastive language-image pretraining. In *Proceedings of the Computer Vision and Pattern Recognition Conference*, pages 9549–9558, 2025.

Mingjin Zhang, Yuanjun Ouyang, Fei Gao, Jie Guo, Qiming Zhang, and Jing Zhang. Mocid: Motion context and displacement information learning for moving infrared small target detection. In *Proceedings of the AAAI Conference on Artificial Intelligence*, volume 39, pages 10022–10030, 2025.

Sicheng Zhu, Luping Ji, Jiewen Zhu, Shengjia Chen, and Weiwei Duan. Tmp: Temporal motion perception with spatial auxiliary enhancement for moving infrared dim-small target detection. *Expert Systems with Applications*, 255:124731, 2024.